Parabolic Procedure for Flows in Ducts with Arbitrary Cross Sections

Donald W. Roberts* and Clifford K. Forester†
Boeing Aerospace Company, Seattle, Wash.

A computer program has been developed to predict three-dimensional compressible viscous flows in ducts with arbitrary cross-sectional shapes. A curvilinear boundary-fitted coordinate system is used to simplify boundary conditions. The parabolized Navier-Stokes equations are transformed, and the solution is marched down the duct using an iterative ADI procedure. Computed results are compared with test data for laminar test cases in square and round ducts. A two-equation turbulence model is demonstrated for a developing turbulent pipe flow. A comparison between predicted results and test data is presented for a turbulent diffuser flow with a rectangular-to-round transition in cross-sectional geometry.

I. Introduction

NUMEROUS examples of flow in ducts of asymmetric cross section are found in aircraft propulsion systems (Fig. 1), particularly in military aircraft. Rectangular or D-shaped inlets that must transform to a circular cross section at the compressor face are found on many fighter aircraft. Integrated two-dimensional nozzles also require a transition of the duct cross-sectional shape. The numerical simulation of the flow through a duct of arbitrary cross section offers potential resource savings over parametric testing and existing data correlation techniques in the design of these propulsion system components by reducing the extent of experimental studies. This could lead to an analysis oriented design approach as opposed to the traditional test-based approach.

Numerical solutions for flows in ducts with arbitrary cross sections require that the three-dimensional Navier-Stokes equations must be solved to simulate the coupling between inertial and viscous effects correctly. This implies that significant amounts of computer time and storage may be required. Previous numerical procedures[1-5] have analyzed flows in ducts with regular cross-section shapes (such as circular or rectangular). A fundamental difficulty with computations in arbitrarily shaped regions is the compatibility of the computational mesh with the boundary conditions. The numerical procedure presented here was designed to circumvent this problem. Background physical and numerical considerations for the design of the duct flow analysis are discussed in Sec. II and the details for the present code are discussed in Sec. III. Validation test case predictions are presented in Sec. IV.

II. Considerations for the Analysis of Duct Flows

Physical Considerations

When considering the types of flows that can occur in ducts, it becomes clear that these flows can be extremely complex. Duct flows can be incompressible or compressible and laminar or turbulent, and significant swirl and crossflow reversal may be present. An example of a complex duct flow is a jet engine exhaust nozzle system. The flow leaving the turbine contains a residual swirl that interacts with support struts and results in the generation of local secondary swirl flows. Geometry and other influences can attenuate or intensify the size and strength of these vortices. These vortices are imbedded in the bulk swirling flow and can interact to cause major distortions in the flowfield. Other secondary flows, particularly those driven by pressure gradients or turbulence, can be found in ducts. The general duct flow might have large gradients in vorticity, mass density, temperature, or chemical species. Furthermore, discontinuities such as shocks, contact surfaces, etc., can exist. Finally, regions of streamwise separation and reattachment may occur.

Many ducts of practical interest can have cross sections of arbitrary shape that transform from one shape to another along the duct. The curvature of the walls and duct centerline is known to have a strong effect on the development of the flow. Obstructions such as centerbodies and plugs can also have an important effect on the duct flowfield. The complexity of the general duct flow problem offers a significant challenge to computational fluid mechanics.

Code Design Considerations

The accuracy and efficiency with which the various flow phenomena are simulated depends directly on the choice of mathematical formulation and on the design of the numerical solution procedure. During the planning stages of the

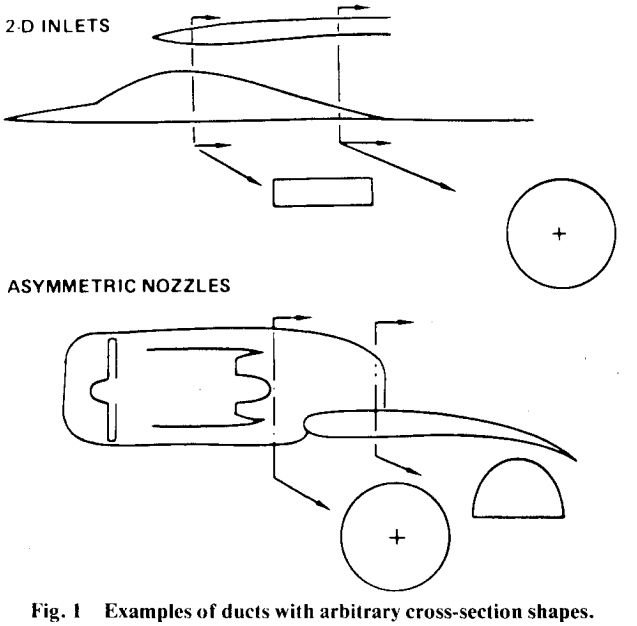

Fig. 1 Examples of ducts with arbitrary cross-section shapes.

Presented as Paper 78-143 at the AIAA 16th Aerospace Sciences Meeting, Huntsville, Ala., Jan. 16-18, 1978; submitted Feb. 13, 1978; revision received Aug. 8, 1978.

Index category: Computational Methods.

*Senior Engineer.

†Specialist Engineer.

development of a computer code, an attempt to achieve a balance between the cost to develop a code and the cost to use a code must be considered. Emphasis in either category may result in inefficient use of man and computer resources. A survey of the literature[6-22] made from this viewpoint led to the following conclusions which were used in the design of the present computer code.

1) While multistep schemes may have efficiency benefits, an implicit scheme that involves only two simultaneous planes of data to implement a marching scheme is a good compromise between simplicity and efficiency.

2) In many applications of interest it is expected that the interaction of the diffusion terms, the convection terms, and the turbulence model of the system of equations requires an implicit scheme for efficiency. ADI (alternating direction implicit) iteration is used to implement the implicit marching scheme. This type of scheme also avoids the errors from splitting as discussed by Fromm.[6] In many cases the Courant number must be restricted to the order of unity to control stepwise truncation errors. In view of this, the implicit approximate factorization schemes[5,7] were deemed to be not cost effective.

3) In duct flows and in computational fluid mechanics in general, the inertially dominated flows are the most difficult to accurately and efficiently simulate numerically. It has been shown[8,9] that such cases are treated most efficiently by fourth- and higher-order accurate convective difference schemes. In certain situations[10-13] additional benefits result from having the scheme conserve kinetic energy. A Crank-Nicholson scheme will conserve kinetic energy and requires just two computational planes for a marching step.[11,12,14-16] The present code has been designed such that a fourth-order accurate Crank-Nicholson-type scheme can be readily incorporated with minimal coding modifications.

4) Computational noise results from the interactions of amplitude errors, phase errors, and Gibbs effect errors[7,11,12,17-20] in convective difference schemes. The noise is manifested in various forms, ranging from substantial nonphysical oscillations to the generation of spurious vortices.[17] Nonlinear filtering[17-19] has been demonstrated to be effective in controlling computational noise. Wavelength filtering was implemented in the current code to deal with this difficulty.

5) Efficient use of grid arrangements requires convenient means for proper mesh placement to resolve the flow details of interest. Self-adaptive body-fitted meshes and mesh clustering schemes have the potential for improved computational efficiency.

6) The selected turbulence model must be validated for the classes of flow types which are expected to be encountered by the analysis if reliable predictive capability is to be achieved.

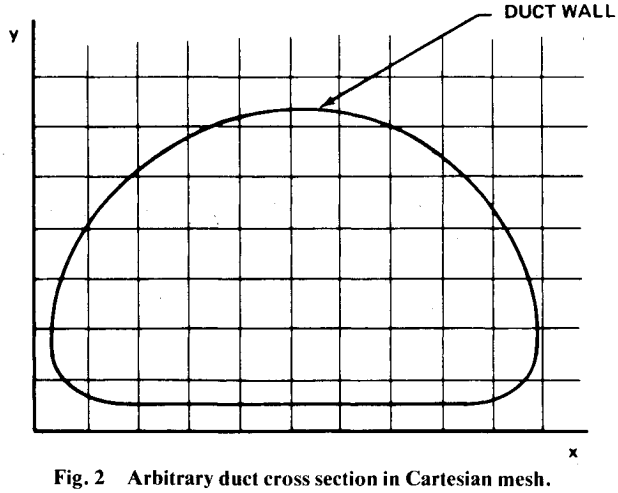

Fig. 2 Arbitrary duct cross section in Cartesian mesh.

III. Development of Present Duct Code

The duct code to be discussed in the following sections is a first step in the development of a more general duct flow analysis. The present analysis is based on the fact that many duct flows can be categorized as parabolic. As discussed by Patankar and Spalding,[1] parabolic flows have a predominant direction of flow. Downstream properties have a negligible influence on the upstream flow; thus, a marching procedure can be used. The unique feature of the present analysis is the use of a boundary-fitted coordinate system that allows an efficent prediction of a certain class of flows in ducts with arbitrary cross sections. This coordinate system is simplified by aligning the transverse computational planes (cross sections) so that they are parallel. This approach limits the duct shapes to those in which the mean centerline is not deflected radically from a straight line even though the duct walls may be subject to substantial distortions.

Boundary-Fitted Computational Mesh

Typical orthogonal meshes, such as the Cartesian form, are difficult to use because the mesh points do not naturally fall on the duct boundaries as shown in Fig. 2. The resulting differencing and interpolation schemes become quite complex and cumbersome, and it is extremely complicated to extend these schemes to higher order with little hope for improved accuracy and efficiency.

Potentially, high-accuracy solutions are possible for the duct of arbitrary cross-section problem when a boundary-fitted computational mesh is employed. By that it is meant that the boundary (duct wall) is coincident with the mesh points that are used for finite-difference expressions at, and adjacent to, the boundary. Interpolation is not required, and extension to higher-order differencing is straightforward. This is a significant benefit when the boundary conditions have a dominant influence on the solution. Thompson et al.[21] and Chu[22] have demonstrated methods for automatically generating boundary-fitted meshes that can be extended to the arbitrary duct problem.

Starting with an arbitrary lateral cross section of a duct in the physical x,y plane (z is the predominant flow direction), a boundary-fitted mesh is generated such that the mesh lines are the coordinates of the ξ,η coordinate system.[21] One of the η-coordinate lines is specified to be coincident with the duct wall. The internal ξ and η coordinates can be calculated by solving an elliptic boundary value problem with Dirichlet boundary conditions. The elliptic mesh-generating equations are transformed and numerically solved in the computational plane.[21] In the computational plane the ξ,η-coordinate system is specified to be rectangular, the mesh is uniform, and the duct wall transforms to a straight coordinate line. Hence, the numerical differencing scheme is straightforward.

The transformation of any differential equation from the physical domain (x,y,z) to the computational domain (ξ,η,σ) is achieved by the following transformation relations[23]:

$$f_x = \frac{\partial(f,y,z)}{\partial(\xi,\eta,\sigma)} \Big/ J \tag{1a}$$

$$f_y = \frac{\partial(x,f,z)}{\partial(\xi,\eta,\sigma)} \Big/ J \tag{1b}$$

$$f_z = \frac{\partial(x,y,f)}{\partial(\xi,\eta,\sigma)} \Big/ J \tag{1c}$$

where $J=\partial(x,y,z)/\partial(\xi,\eta,\sigma)$ is the Jacobian of the transformation. Higher derivative are found by repeated use of Eqs. (1).

Since the duct cross-sectional planes are parallel and specified to be x,y planes, the two-dimensional equivalent of Eqs. (1) is used to transform the system of elliptic mesh-

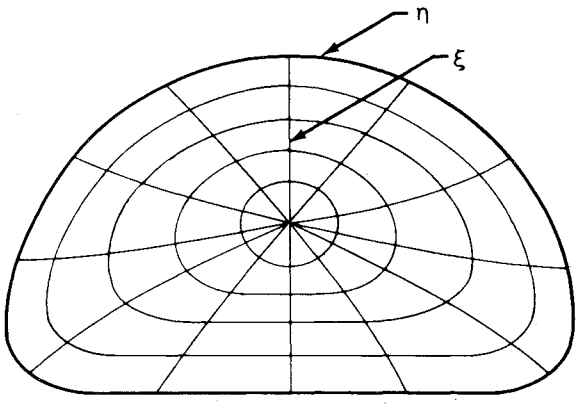

Fig. 3 Boundary-fitted mesh plotted in x, y plane.

generating equations, yielding[21]:

$$Ax_{\xi\xi} - 2Bx_{\xi\eta} + Cx_{\eta\eta} + J^2(Rx_\xi + Qx_\eta) = 0 \tag{2a}$$

$$Ay_{\xi\xi} - 2By_{\xi\eta} + Cy_{\eta\eta} + J^2(Ry_\xi + Qy_\eta) = 0 \tag{2b}$$

where $A = x_\eta^2 + y_\eta^2$, $B = x_\xi x_\eta + y_\xi y_\eta$, and $C = x_\xi^2 + y_\xi^2$.

The values of x and y corresponding to the duct wall are specified on an η-coordinate line. This sytem of quasilinear equations is solved using line overrelaxation. The solution yields values of x and y which become the computational mesh points. A one-to-one mapping performs the reverse transformation and yields the solution for ξ and η in the physical plane (Fig. 3). A singularity point appears for the ξ,η mesh in the physical plane. This does not present a problem for the mesh-generating equations, as it can be treated as a Dirichlet boundary condition. The treatment of this point for the flow equations is deferred until a later section.

The three-dimensional mesh for the parabolic duct flow analysis can be viewed as a series of two-dimensional meshes generated for each x,y cross-sectional plane. As the solution is marched from plane to plane, each cross section is transformed to a straight line in the computational plane. All computational planes contain an equal number of mesh points which form identical uniform meshes. The three-dimensional mesh is formed by connecting adjacent upstream and downstream mesh points. Care is taken to prevent significant skewing of the mesh from plane to plane, and all of the three-dimensional metric information is retained in the flow equations. In practice the computational mesh at downstream planes is not generated until it is required.

A significant benefit of using a numerical mesh generator is the automated control one has over the mesh density using the functions R and Q which appear in Eq. (2). These are functions of ξ and η which allow the possibility of optimally distributing the computational mesh.[21] By using suitable functions, the mesh can be contracted towards areas of special interest such as the duct wall. Eventually, functional relationships should be developed such that regions of steep gradients in the flow properties can be tracked by the mesh. This efficient use of the available mesh points offers the potential for major reductions in the use of computer time and storage.

Transformed Flow Equations

Using the parabolic approximations, the Navier-Stokes equations are parabolized by neglecting the streamwise diffusion terms and by decoupling the streamwise and lateral plane pressure gradients. The streamwise pressure gradient is assumed to be constant across a duct cross section. The parabolic approximation allows the use of a marching procedure.

The Cartesian primitive variable form of the parabolized Navier-Stokes equations are transformed using Eq. (1) such that they can be solved in the computational plane and benefit from the boundary-fitted computational mesh. An appreciable simplification of the transformed flow equations is realized by assuming that the duct cross sections are parallel and perpendicular to the z coordinate. Then z_ξ and z_η are zero and z_σ is a constant.

In ξ,η,σ coordinates, the steady, three-dimensional continuity, momentum, and energy equations are given by the following:

$$(y_\eta \rho u)_\xi - (y_\xi \rho u)_\eta + (x_\xi \rho v)_\eta - (x_\eta \rho v)_\xi + (D\rho w)_\xi + (E\rho w)_\eta + [(J/z_\sigma)\rho w]_\sigma = 0 \tag{3a}$$

$$Fu_\xi + Gu_\eta + (J\rho w/z_\sigma)u_\sigma + y_\eta P_\xi - y_\xi P_\eta = S \tag{3b}$$

$$Fv_\xi + Gv_\eta + (J\rho w/z_\sigma)v_\sigma + x_\xi P_\eta - x_\eta P_\xi = S \tag{3c}$$

$$Fw_\xi + Gw_\eta + (J\rho w/z_\sigma)w_\sigma + \bar{P}_z = S \tag{3d}$$

$$FH_\xi + GH_\eta + (J\rho w/z_\sigma)H_\sigma = S \tag{3e}$$

where

$$D = \frac{x_\eta y_\sigma - x_\sigma y_\eta}{z_\sigma}, \qquad E = \frac{y_\xi x_\sigma - x_\xi y_\sigma}{z_\sigma}$$

$$F = y_\eta \rho u - x_\eta \rho v + D\rho w, \qquad G = -y_\xi \rho u + x_\xi \rho v + E\rho w,$$

$$J = x_\xi y_\eta - x_\eta y_\xi$$

and S represents the appropriate diffusion terms where applicable; however, they are too cumbersome to write here. The Cartesian velocity components u, v, and w have been retained. The $\bar{P}_z$ which appears in the w-momentum equation represents a constant streamwise pressure gradient for a given cross section. H is the total enthalpy. The fluid is assumed to be calorically perfect, and an equation of state is used to calculate density ρ.

The primary function of the streamwise and lateral plane pressure gradients is to insure that continuity is preserved. The streamwise pressure gradient $\bar{P}_z$ is calculated from an auxiliary relation which in simplest terms compares the predicted mass flow rate with the known flow rate and adjusts $\bar{P}_z$ such that mass is conserved.[1] Iteration with the w-momentum equation is required until the predicted mass flow rate reaches a specified level of accuracy. Thus, the overall continuity is satisfied.

Local continuity is satisfied by means of the lateral plane pressure gradients. Thus, Eq. (3a) is solved indirectly. The pressure field P is calculated by solving an elliptic equation which is derived by taking the divergence of the u- and v-momentum equations. This results in

$$AP_{\xi\xi} - 2BP_{\xi\eta} + CP_{\eta\eta} + J^2(RP_\xi + QP_\eta) = S + (Jw/z_\sigma)\mathfrak{D}_\sigma \tag{4}$$

S represents the contribution of the convection and diffusion terms, and $\mathfrak{D}$ is the continuity variable. For clarity $\mathfrak{D}$ is multiply defined by the following:

$$\mathfrak{D}_{cs} = (y_\eta \rho u)_\xi - (y_\xi \rho u)_\eta + (x_\xi \rho v)_\eta - (x_\eta \rho v)_\xi \tag{5a}$$

$$\mathfrak{D}_{sw} = -[(D\rho w)_\xi + (E\rho w)_\eta + (J\rho w)_\sigma / z_\sigma] \tag{5b}$$

where $\mathfrak{D}_{cs}$ is the lateral plane component of continuity and $\mathfrak{D}_{sw}$ is the streamwise component as determined from Eq. (3a). The significance of the $\mathfrak{D}_\sigma$ term in Eq. (4) warrants a detailed discussion of its discretization to be presented in the next section.

Discretization and Boundary Conditions

All equations are transformed to finite-difference form by standard second-order centered difference approximations for ξ and η derivatives and by one-sided upstream differences for σ derivatives. Where needed, diffusion coefficients between mesh points are formed from simple averages of adjacent mesh point values. By experimentation it was found that weighting the coefficients that varied rapidly in Eqs. (3) between the upstream and downstream planes resulted in improved accuracy and stability. This only affects the stepwise truncation error, and the weighting effects can be negated by suitable step size constraints.

The treatment of $\mathfrak{D}_\sigma$, Eq. (4), requires special consideration. In discrete form $\mathfrak{D}_\sigma$ becomes

$$\mathfrak{D}_\sigma = (\mathfrak{D}^{n+1} - \mathfrak{D}^n)/\Delta\sigma \tag{6}$$

where $n+1$ and n represent two adjacent duct cross sections. $\mathfrak{D}^{n+1}$ is calculated from the discrete form of $\mathfrak{D}_{sw}$ at the downstream plane, which has a low level of error since w is accurately controlled by the $\bar{P}_z$ iteration procedure discussed earlier. $\mathfrak{D}^n$ could be evaluated from $\mathfrak{D}_{sw}$ at the upstream plane. However, improved results are achieved by the use of the discrete form of $\mathfrak{D}_{cs}$ for $\mathfrak{D}^n$. This is related to the procedure developed by Harlow and Welch[24] and equivalent to the procedure used by Forester.[25] The main benefit of this approach is the dramatic accuracy improvements which result for problems in which continuity cannot easily be satisfied for the initial conditions.

No slip boundary conditions are enforced in the present analysis. The three velocity components u,v, and w are set to zero on the duct walls. The pressure equation has a Neumann boundary condition. An expression for the pressure gradient normal to the wall is obtained by manipulating the u- and v-momentum equations. An adiabatic wall boundary condition is used with the energy equation. Wall functions model the turbulence quantitites near the wall.[26]

The singularity point discussed in the previous section does not present a problem for the solution of the flow equations. Analytically, the metrics vanish at this point and the flow variables become multivalued; however, this point can be treated numerically. The primary concern is that the flowfield is allowed to communicate accurately through the inner mesh point when required. In the present duct analysis, metrics are generated at the singularity point by using the surrounding mesh points. The flow equations are solved explicitly at this point for each ξ line at the end of an iteration. This multivalued solution is averaged to obtain values of the flow variables at the inner mesh point. In practice, the multivaluedness of the solution vanishes when the local Courant number is less than unity, and the solution is constant to within six decimal places. Small phase errors may be introduced by this method, but they should not be substantial in comparison to those generated by the numerical algorithm in the field mesh.

Turbulence Model

Closure of the set of flow equations for turbulent flow is achieved by modeling the Reynolds stresses that appear in the time-averaged Navier-Stokes equations. The present analysis incorporates an energy-dissipation turbulence model, a form of which was first proposed by Harlow and Nakayama.[27] Launder and Spalding[26] have demonstrated this two differential equation model, which is solved for the turbulence energy k and its dissipation rate ϵ, for a wide range of flows. This model uses the eddy viscosity concept with the eddy viscosity μ_τ calculated from the following relation:

$$\mu_\tau = C_\mu \rho k^2/\epsilon \tag{7}$$

The two coupled differential equations used to predict k and ϵ have the same form as Eq. (3e) with the exception that the right-hand side contains additional source terms representing the effects of production and dissipation. A general discussion of this turbulence model will not be presented here since adequate documentation of its effectiveness for a variety of flows is available.[26,28]

Numerical Noise Filter

Since the numerical algorithm chosen for the present analysis is formally second order, it is subject to computational noise that can arise in steep gradient regions of the flowfield. To control the computational noise, which can overwhelm a solution, a noise filter has been incorporated.

The filter chosen is conceptually the same as that developed by Forester.[17] The filter examines the solution domain and removes noise when it is identified. This type of filter is preferable to methods that globally add artificial viscosity to control noise, since those methods will also damp regions of the solution that are not plagued by noise. Our selective filter only affects noisy regions. The mechanism for identifying the computational noise is based on the noise wavelength. The filter can be designed to look for noise of various wavelengths, where the minimum wavelength is two mesh intervals. The maximum wavelength that must be filtered depends on the order of the numerical scheme and the type of flow being simulated. The filter currently in use searches for noise with wavelengths of two and four mesh intervals. This has proved to be sufficient to eliminate noise and maintain stability in flows with high cell Reynolds numbers.

Solution Procedure

A marching solution procedure is used. A solution is obtained at each duct cross section before a step is taken downstream to the next lateral plane. Mesh-generating Eqs. (2) and the lateral plane pressure Eq. (4) are solved using line overrelaxation (LOR). The solution for the nonlinear flow equations is achieved by iterating with an ADI scheme at each downstream plane until a suitable convergence is obtained.

Given an initial set of data in the starting plane, the program uses the following sequence to obtain a solution at the next plane: 1) Generate computational mesh; 2) advance w-momentum equation, insure mass conservation by iteratively adjusting the axial pressure gradient; 3) advance u- and v-momentum equations to obtain tentative u and v; 4) solve lateral plane pressure equation; 5) update u- and v-momentum equations using corrected pressure gradients; 6) advance energy equation and calculate density; 7) advance turbulence model equations.

Steps 2-7 are iterated to reduce the accumulation of truncation errors that can result from linearization. Without iteration, a converged solution is not obtained at each plane and accuracy is compromised. The amount of iteration required depends on the rate at which the flow is changing axially in the duct. Typically, a couple of iterations are sufficient.

IV. Computational Results

Several computational experiments have been run for assessing the accuracy and stability of the present numerical procedure and to test the suitability of the described general transformation for flows in ducts with arbitrary cross sections. Laminar test cases were run initially; then the turbulence model was activated and checked out.

Laminar Test Cases

Laminar constant viscosity flows provide a useful means for analyzing the numerics, since it is often possible to find experimental and other analytical data for comparison. The two cases presented here represent developing laminar flows in the inlet regions of constant cross-section ducts. The first duct to be analyzed was a round pipe; the second had a square cross section. A uniform initial velocity profile was used. The Reynolds number, based on the mean velocity $\bar{u}$ and the duct

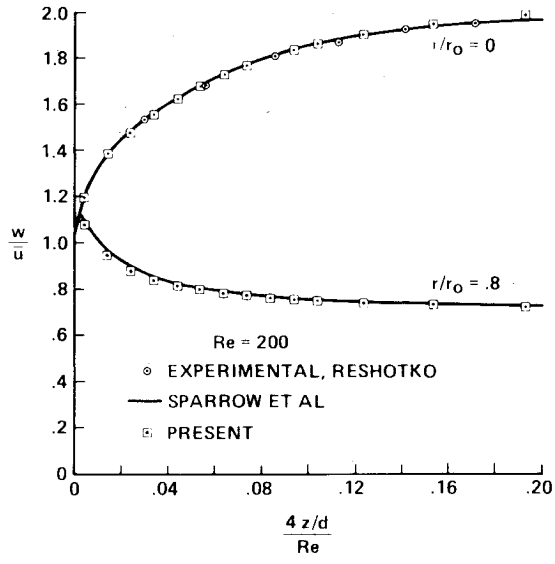

Fig. 4 Streamwise velocity development at two radial positions for laminar flow in a circular duct with radius, r_0.

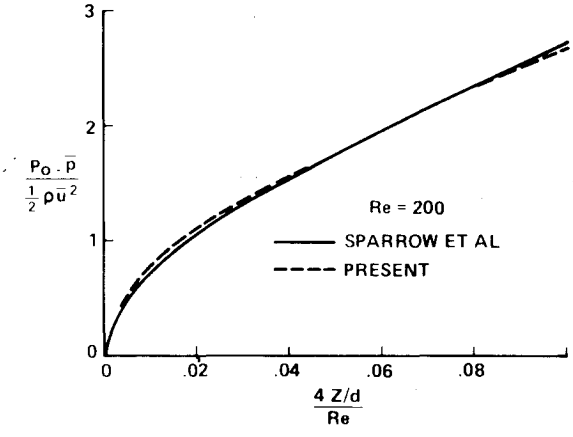

Fig. 5 Prediction of pressure drop for developing laminar flow in a circular duct.

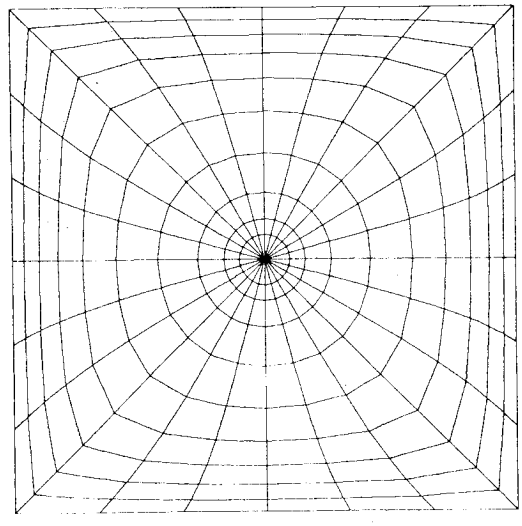

Fig. 6 Boundary-fitted mesh for laminar square duct flow.

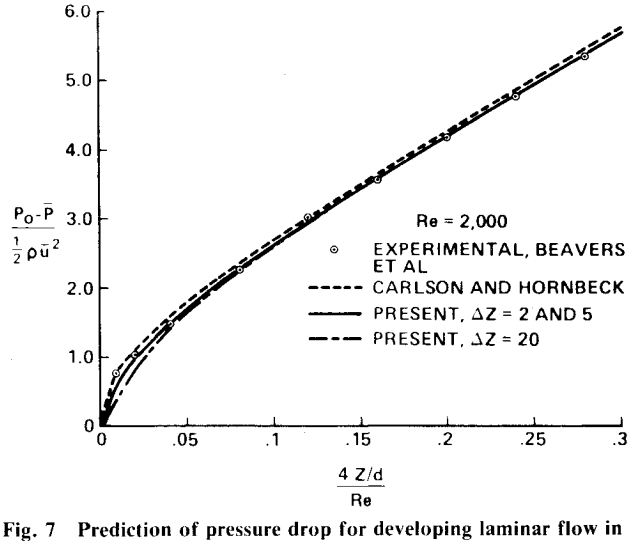

Fig. 7 Prediction of pressure drop for developing laminar flow in a square duct.

diameter d was varied from 8 to 2000. For the developing laminar pipe inlet case, the results are presented at Reynolds number $Re = 200$. In Fig. 4, the predictions of the axial velocity are compared with the analysis of Sparrow et al.[29] and the experimental data of Reshotko.[30] The pressure drop in the inlet region is shown in Fig. 5.

The results for the square cross-section duct are presented for $Re = 2000$ and are compared with the experimental data of Beavers et al.[31] and the analysis of Carlson and Hornbeck.[32] The boundary-fitted computational mesh for this case was slightly contracted towards the duct wall (see Fig. 6). Three streamwise step sizes, Δz (where Δz is normalized by the duct half-width), were used to determine when stepwise truncation errors become significant. The pressure drop predictions are shown in Fig. 7. A favorable comparison with the experimental data for both $\Delta z = 2$ and 5 exists, whereas $\Delta z = 20$ yields predictions that miss the initial transient region where the streamwise gradients are most severe. The number of lateral plane mesh points used in the present analysis is a factor of 3 less than that required by the equivalent Carlson and Hornbeck scheme. This can be attributed to the distribution of the mesh near the wall. In the present predictions, the contracted mesh yielded a mesh density in the steep gradient region of the wall equal to that used by Carlson and Hornbeck. Away from the wall, the mesh density was gradually decreased, thus requiring fewer mesh points. This clearly demonstrates the benefit of optimally distributing the mesh.

To examine the effectiveness of the method used to handle the mesh singularity point, a test case was run for the laminar pipe at $Re = 200$ with the singularity point moved two-tenths of a radius off the duct axis. With the point in this position, the crossflow passes through it. A converged solution was obtained for all flow variables at the singularity point for each z station along the duct. As shown in Fig. 8, the predictions of the velocity profile with and without the singularity point on the duct axis show excellent agreement. Any irregularities are due to the nonsymmetry of the mesh about the axis. The pressure drop predictions are virtually identical to those shown in Fig. 5.

Turbulent Test Cases

The turbulence model discussed earlier was checked out by predicting a fully developed turbulent flow in a round pipe. This is one test case for which reliable experimental data are available. A uniform initial velocity profile was specified. The Reynolds number was 1.4×10^5. The predictions indicate that the fully developed turbulent velocity profile evolves at 40-50 pipe diameters, but that the turbulence quantities are not fully developed until 75-100 diameters. This agrees with the information discussed in Schlichting.[33] The predicted fully developed velocity, turbulence kinetic energy,

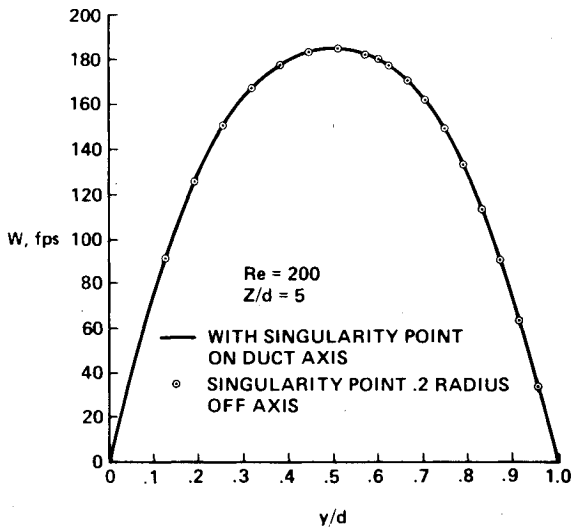

Fig. 8 Laminar velocity profile with and without mesh singularity point on the duct axis.

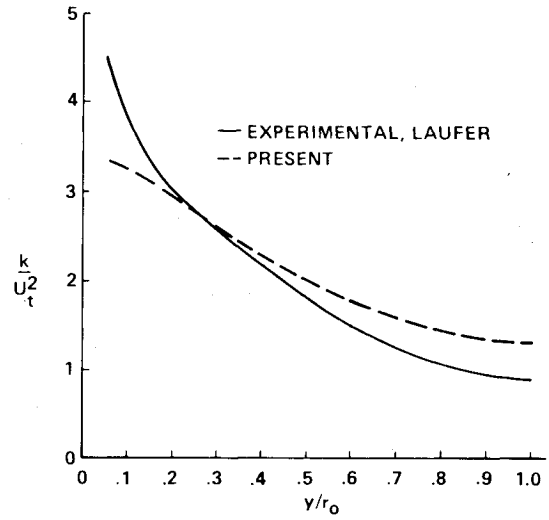

Fig. 10 Fully developed turbulent kinetic energy profile in a circular duct.

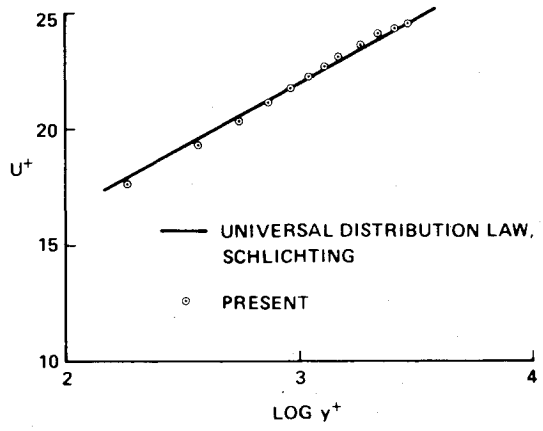

Fig. 9 Fully developed turbulent velocity profile in a circular duct.

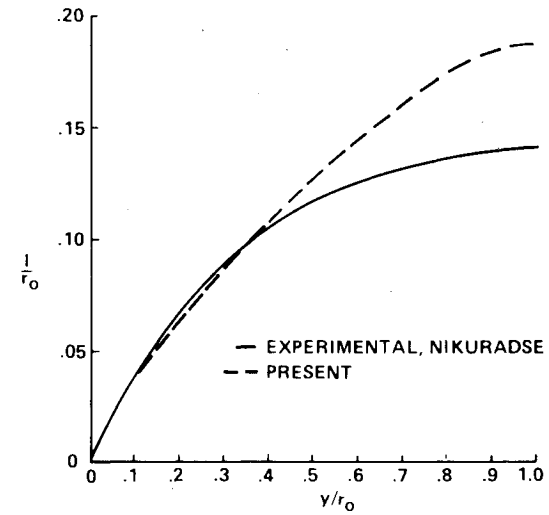

Fig. 11 Fully developed length scale profile in a circular duct.

and turbulent length scale profiles are presented in Figs. 9-11. The agreement with the experimental data[33,34] is favorable. The deviation of the predicted length scale near the duct axis is probably a result of the fact that the constants in the turbulence model diffusion terms were based on near wall turbulence. Since the gradients near the axis are small, this lack of agreement was inconsequential.

The k-ϵ turbulence model is not capable of predicting the turbulence-driven secondary flows that are generated in noncircular ducts. These secondary flows are not likely to be relevant in aircraft applications because there are few practical cases in which the noncircular ducts are straight for a long enough distance.[35] However, the model is very useful for predicting turbulent boundary layers and flows that involve the mixing of two different streams.[28]

Three-Dimensional Flow Prediction

While the preceding test flows were three-dimensional because all three velocity components were present, the geometries were of little interest except for evaluating the numerical procedure. In practice, there are little detailed experimental data available for flows in ducts with arbitrary cross sections. One set of experiments in which some mean flow quantities were measured is reported by MacMiller.[36] The ducts in this investigation were subsonic diffusers similar to those found in supersonic inlets. The case chosen is for the flow in the diffuser illustrated in Fig. 12. This diffuser has a rectangular entrance and immediately begins to transform in shape until a circular cross section is reached at the simulated engine face. The diffuser angles become quite large, and the experimentalists indicate that separation was evident at approximately 50% of the diffuser length. The data for this case consist of the static pressure distribution and measurements of the total pressure profiles along the minor axes of the duct cross sections at several axial locations indicated in Fig. 12.

Upstream of the diffuser entrance the flow has gone through a strong shock and a boundary-layer bleed region which distort the boundary-layer profile. The initial conditions at the diffuser entrance consisted of a core flow at a Mach numer of $M = 0.605$ and a uniform boundary-layer thickness of ½ in. In view of the lack of a detailed experimental description of the boundary-layer profile, it was simulated with power law exponents of 3, 5, and 7. The sensitivity of the results to the initial conditions was ascertained in this manner. To insure that our numerical results were not a function of the number of mesh points, a mesh refinement study was performed. The differences in the predicted results for the coarse mesh and the finest mesh, which was factor of 4 denser, were less than 1 %.

The prediction of the static pressure rise in the diffuser is compared with the experimental data in Fig. 13. Separation was indicated in the computed results by negative w-velocity components after which the computation is halted. The numerical separation point does agree quite well with that indicated by the test data regardless of the initial boundary-

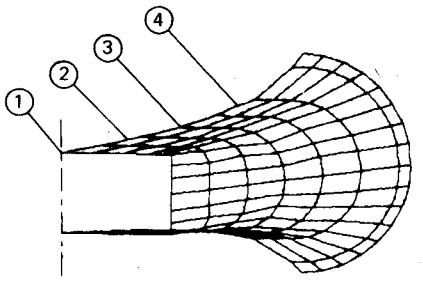

Fig. 12 Three-dimensional computer plot of rectangular-round diffuser.

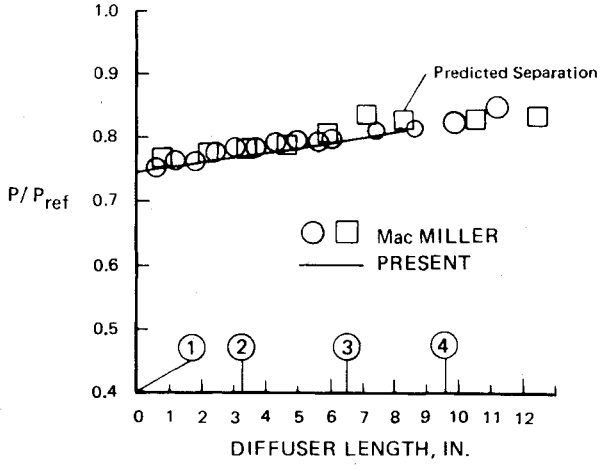

Fig. 13 Static pressure rise for rectangular-round diffuser.

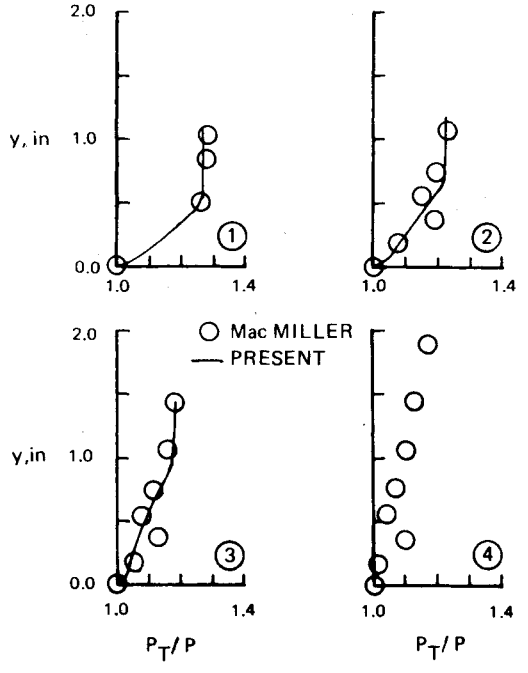

Fig. 14 Measured and predicted total pressure profiles.

layer profile. A more detailed view of the profile distortion that leads to separation is presented in Fig. 14 for a power law exponent of 3. With this choice the agreement with the experimental data is good, with the exception of one data point that appears to be bad since it does not follow the trend of the other data. An exponent of 3 indicates a very distorted profile which is to be expected given the upstream flow conditions.[37]

V. Conclusions

A finite-difference numerical procedure has been developed for the prediction of parabolic flows in ducts with arbitrary cross sections. The analysis features a boundary-fitted computational mesh with external control of the mesh density. The flow equations are transformed using a general curvilinear transformation. The decoupled streamwise and lateral plane pressure gradients are controlled to enforce mass continuity. A two-equation turbulence model has been incorporated for turbulent flows. A selective computational noise filter is used to eliminate spurious solutions. Good agreement was obtained between predicted and measured flow properties for a turbulent diffuser flow with a rectangular-to-round transition in cross-section geometry.

References

[1] Patankar, S.V. and Spalding, D.B., "A Calculation Procedure for Heat, Mass, and Momentum Transfer in Three-Dimensional Parabolic Flow," *International Journal of Heat and Mass Transfer*, Vol. 15, 1972, pp. 1787-1806.

[2] Ghia, U., Ghia, K.N., and Studerun, C.J., "A Study of Three-Dimensional Laminar Incompressible Flow in Ducts," AIAA Paper 76-424, 1976.

[3] Briley, W.R., "Numerical Method for Predicting Three-Dimensional Steady Viscous Flows in Ducts," *Journal of Computational Physics*, Vol. 14, 1974, pp. 8-28.

[4] Patankar, S.V., Pratap, V.S., and Spalding, D.B., "Prediction of Laminar Flow and Heat Transfer in Helically Coiled Pipes," *Journal of Fluid Mechanics*, Vol. 62, 1974, pp. 539-551.

[5] Briley, W.R. and McDonald, H., "Solution of the Multidimensional Compressible Navier-Stokes Equations by a Generalized Implicit Method," *Journal of Computational Physics*, Vol. 24, 1977, pp. 372-397.

[6] Fromm, J.E., "A Numerical Method for Computing the Non-Linear, Time Dependent, Bouyant Circulation of Air in Rooms," IBM Research, San Jose, Calif., RJ732, July 28, 1970.

[7] Beam, R.M. and Warming, R.F., "An Implicit Finite-Difference Algorithm for Hyperbolic Systems in Conservation-Law Form," *Journal of Computational Physics*, Vol. 22, Sept. 1976, pp. 87-110.

[8] Rubin, S.G. and Khosla, P.K., "Polynomial Interpolation Methods for Viscous Flow Calculation," *Journal of Computational Physics*, Vol. 24, July 1977, pp. 217-224.

[9] Kreiss, H.O. and Oliger, J., "Comparison of Accurate Methods for the Integration of Hyperbolic Equations," *Tellus*, Vol. 24, 1972, pp. 199-215.

[10] Arakawa, A., "Numerical Simulation of Viscous Incompressible Flow," *Numerical Solution of Field Problems in Continuum Physics*, 24, American Mathematical Society, Providence, R.I., 1970, pp. 281-317.

[11] Orszag, S.A., "Numerical Simulation of Incompressible Flows Within Simple Boundaries: Accuracy," *Journal of Fluid Mechanics*, Vol. 49, 1971, pp. 75-112.

[12] Williams, G.P., "Numerical Integration of the Three-Dimensional Navier-Stokes Equations for Incompressible Flow," *Journal of Fluid Mechanics*, Vol. 37, 1969, pp. 272-750.

[13] Piacsek, S.A. and Williams, G.P., "Conservation Properties of Convection Difference Schemes," *Journal of Computational Physics*, Vol. 6, 1970, pp. 392-405.

[14] Forester, C.K., Patterson, H.W., and Barton, J.E., "Computer Program Manual—Cyrogenic Tank External Loop Pressurization Analysis," Boeing Document No. D2-118462-1, Contract No. NAS9-12977, Boeing Aerospace Co., Houston, Texas, May 1973.

[15] Morton, K.W., "Stability and Convergence in Fluid Flow Problems," *Proceedings of the Royal Society London A*, Vol. 323, 1971, pp. 237-253.

[16] Gazdag, J., "Numerical Convective Schemes Based on Accurate Computation of Space Derivatives," *Journal of Computational Physics*, Vol. 13, 1973, pp. 100-113.

[17] Forester, C.K., "Higher Order Monotonic Convective Difference Schemes," *Journal of Computational Physics*, Vol. 23, Jan. 1977, pp. 1-22.

[18] Van Leer, B., "Towards the Ultimate Conservative Difference Scheme. II. Monotonicity and Conservation Combined in a Second-Order Scheme," *Journal of Computational Physics*, Vol. 14, 1974, pp. 361-370.

[19] Boris, J.P. and Book, D.L., "Minimizing Errors in Flux-Corrected Transport Algorithms," Naval Research Lab, Memorandum Rept. 3024, April 1975.

[20] Roberts, K.V. and Weiss, N.O., "Convective Difference Schemes," *Mathematics of Computation*, Vol. 20, 1966, pp. 272-299.

[21] Thompson, J.F., Thames, F.C., and Mastin, C.W., "Automatic Numerical Generation of Body-Fitted Curvilinear Coordinate System for Field Containing Any Number of Arbitrary Two-Dimensional Bodies," *Journal of Computational Physics,* Vol. 15, 1974, pp. 299-319.

[22] Chu, W.H., "Development of a General Finite Difference Approximation for a General Domain—Part I: Machine Transformation," *Journal of Computational Physics,* Vol. 8, 1971, pp. 392-408.

[23] Hildebrand, F.B., *Advanced Calculus for Engineers,* Prentice-Hall, Englewood Cliffs, N.J., 1960, p. 359.

[24] Harlow, F.H. and Welch, J.E., "Numerical Calculation of Time-Dependent Viscous Incompressible Flow of Fluid with Free Surface," *The Physics of Fluids,* Vol. 8, Dec. 1965, pp. 2182-2189.

[25] Forester, C.K. and Emery, A.F., "A Computational Method for Low Mach Number Unsteady Compressible Free Convective Flows," *Journal of Computational Physics,* Vol. 10, 1972, pp. 487-502.

[26] Launder, B. and Spalding, D.B., "The Numerical Computation of Turbulent Flows," *Computer Methods in Applied Mechanics and Engineering,* Vol. 3, 1974, pp. 269-289.

[27] Harlow, F.H. and Nakayama, P., "Transport of Turbulence Energy Decay Rate," Los Alamos Science Lab., Rept. LA-3854, 1968.

[28] Birch, S.F., Paynter, G.C., Spalding, D.B., and Tachtell, D.G., "Numerical Modeling of Three-Dimensional Flows in Turbofan Engine Exhaust Nozzles," *Journal of Aircraft,* Vol. 15, Aug. 1978, pp. 489-496.

[29] Sparrow, E.M., Lin S.H., and Lundgren, T.S., "Flow Development in the Hydrodynamic Entrance Region of Tubes and Ducts," *The Physics of Fluids,* Vol. 7, March 1964, pp. 338-347.

[30] Reshotko, E., Jet Propulsion Laboratory, Rept. No. 20-364, 1958.

[31] Beavers, G.S., Sparrow, E.M., and Magnuson, R.A., "Experiments on Hydrodynamically Developing Flow in Rectangular Ducts of Arbitrary Aspect Ratio," *International Journal of Heat and Mass Transfer,* Vol. 13, 1970, pp. 689-702.

[32] Carlson, G.A. and Hornbeck, R.W., "A Numerical Solution of Laminar Entrance Flow in a Square Duct," *Journal of Applied Mechanics,* March 1973, pp. 25-30.

[33] Schlichting, H., *Boundary-Layer Theory,* 6th ed., McGraw-Hill, New York, 1968, Chap. 20.

[34] Laufer, J., "The Structure of Turbulence in Fully Developed Pipe Flow," NACA Tech. Rept. 1174, 1954.

[35] Bradshaw, P., "Interacting Shear Layers in Turbomachines and Diffusers," *Turbulence in Internal Flows,* edited by S.N.B. Murthy, Project Squid, Office of Naval Research 1977.

[36] MacMiller, C.J., "Investigation of Subsonic Duct Distortion," Air Force Flight Dynamics Lab, Technical Rept. AFFDL-TR-69-21, 1969, pp. 218-221.

[37] Syberg, J. and Koncsek, J.L., "Experimental Evaluation of a Mach 3.5 Axisymmetric Inlet," NASA CR-2563, July, 1975.